RESEARCH PAPER

Synthesis, Characterization, and Anticancer Bioactivity of a Novel Nano-Schiff Base Ligand (NPTIPPE) Derived from 4-Aminoantipyrine and Its Palladium Complex

Ashraf Abdulridha Hussein and Hayder Obaid Jamel *

Department of Chemistry, College of Education, University of Al-Qadisiyah, Diwaniyah, Iraq

ARTICLE INFO

Article History:
Received 17 January 2025
Accepted 14 March 2025
Published 01 April 2025

Keywords:
MCF-7 breast cancer cells
MTT assay
Palladium (II) complexes
Schiff-base nano ligand (NPTIPPE)

ABSTRACT

The novel nano ligand (NPTIPPE) was synthesized *via* a reaction sequence involving benzil, 4-aminoantipyrine, and 2-aminothiazole. Subsequently, the palladium (II) complex was formed by reacting NPTIPPE with palladium chloride in ethanol, maintaining a 1:1 metal:ligand ratio. The nano-ligand and its complex were characterized using various techniques, including NMR, FTIR, UV-Vis spectroscopy, FESEM, and XRD. The ^{1}H-NMR spectrum of NPTIPPE displayed signals corresponding to methyl and phenyl groups, while the ^{13}C-NMR spectrum identified signals associated with the pyrazole and thiazole rings. The FTIR spectra confirmed the presence of azomethine and aromatic groups, with shifts indicating coordination with palladium. The UV-Vis spectra revealed intra-ligand transitions and electronic transitions consistent with a square planar geometry for the palladium (II) complexes. Molar conductivity measurements suggested ionic characteristics. XRD analysis demonstrated differences in crystallite size and dislocation density between the nano ligand and complex. The FESEM images showed distinct morphological differences, reinforcing the structural findings. Biological evaluations using MTT assays on MCF-7 cancer cells and WRL-68 healthy cells indicated that the palladium (II) complexes exhibited higher cytotoxicity against cancer cells as compared to the ligand. The IC50 values for the palladium (II) complex were 87.37 µg/mL for MCF-7 cells and 125.94 µg/mL for WRL-68 cells, suggesting its potential as an effective therapeutic agent against breast cancer.

How to cite this article
Hussein A., Jamel H. Synthesis, Characterization, and Anticancer Bioactivity of a Novel Nano-Schiff Base Ligand (NPTIPPE) Derived from 4-Aminoantipyrine and Its Palladium Complexr. J Nanostruct, 2025; 15(2):608-620. DOI: 10.22052/JNS.2025.02.021

INTRODUCTION

1-phenyl-2,3-dimethylpyrazol-5-one is known as 4-aminoantipyrine or 4-aminophenazone. Pyrazole, a five-membered ring with two nitrogen atoms and a double bond, is important. Its substituted derivatives are biologically active [1, 2]. It also makes ion-selective electrodes [3] and suppresses enzymes [4]. The biological action of 4-aminoantipyrine against bacteria makes it notable. It is a strong analgesic, anti-inflammatory, and fever reducer in circumstances where aspirin is unsuccessful, such as Hodgkin's disease and salicylate-resistant fevers. It also helps identify aromatic chemicals and metal ions utilizing various analytical methods. It helps make antipyrinyl azo

* *Corresponding Author Email: haider.hassani@qu.edu.iq*

dyes, which are essential metal ion colorimetric indicators. Under acidic circumstances, these compounds produce metal chelate complexes. Certain pyrazole compounds have also shown promise against certain cancers [5]. Over 100 types of cancer result from the uncontrolled, fast, and deadly development of abnormal cells in organs and tissues [6, 7]. This disease is caused by DNA mutations in cells, which are organized into many genes with instructions for cellular functioning, growth, and division [7]. Incorrect instructions can cause the cell to stop working, causing numerous malignancies, including breast cancer, the most frequent disease in women after skin cancer [8]. Breast cancer usually starts in the milk-producing ducts (invasive ductal carcinoma), but it can also occur in the lobules or other breast tissues [9]. The new Schiff base ligand (NPTIPPE) generated from 4-aminoantipyrine and a pd (II) complex was synthesized in this study. These compounds were characterised spectroscopically and physically and tested for anticancer efficacy.

MATERIALS AND METHODS

Reagents and instruments

The chemicals used in this study were obtained from Merck, Sigma-Aldrich, and BDH. Breast cancer cell lines (MCF-7) and normal cell lines (WRL-68) were also obtained from the Educational Research Center, Division of Cellular, Molecular, Microbial, and Animal Services / Roshdy Azmeh Company in Tehran. UV-Vis spectra in the range of 200–1000 nm were acquired using a Shimadzu UV-165 PCS spectrophotometer. ^{1}H and ^{13}C-NMR spectra were recorded at a frequency of 300 MHz using tetramethylsilane as an internal standard reference and DMSO-d6 as a solvent. The FTIR spectra were recorded using a Shimadzu FTIR 8400S spectrophotometer in the range of 400-4000 cm^{-1}. Melting points of the nano ligand and the prepared complex were determined using a Stuart melting point apparatus. Magnetic susceptibility measurements at room temperature were performed using a magnetic susceptibility balance model MSB-MKI. Flame atomic absorption spectra were recorded using a Shimadzu AA-6300. Elemental analysis for C, H, and N was conducted using an EA-300 elemental analyzer.

Synthesis procedure

Synthesis of the heterocyclic Schiff base nano ligand (NPTIPPE)

The ligand (NPTIPPE) was synthesized in two steps. The first step involved the preparation of (4-(((2E,3E) -3- (hydroxy imino) butan-2-ylidene) amino) -1,5-dimethyl -2-phenyl- 1,2-dihydro -3H-pyrazol -3 - one (compound-A). This was achieved by reacting benzil (1.05 g, 0.005 mol) in

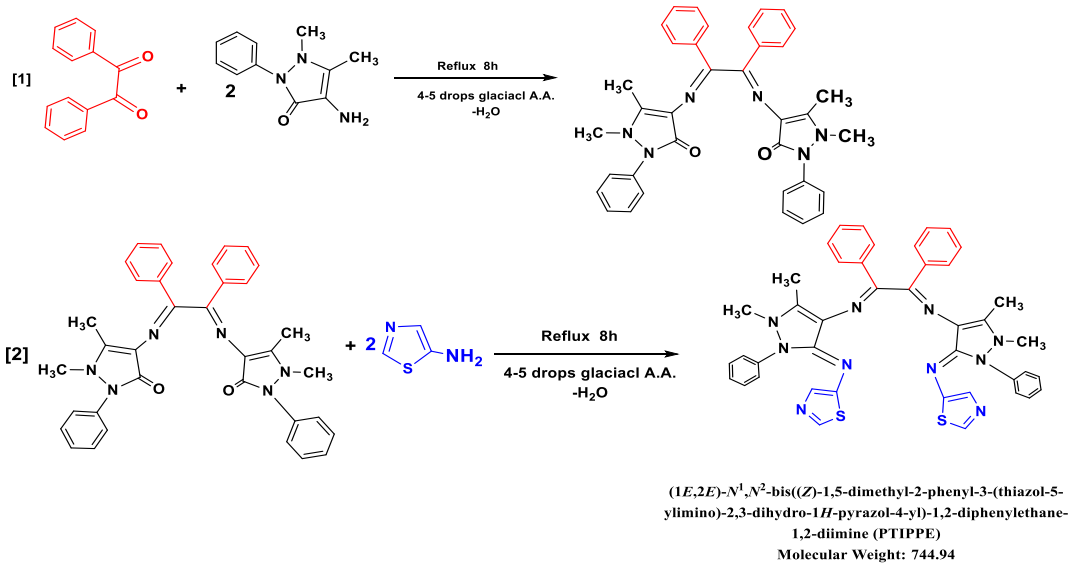

Fig. 1. Scheme for the synthesis of the novel schiff base nano ligand (NPTIPPE) derived from thiazole and salicylaldehyde.

25 mL of absolute ethanol, with the addition of 4-5 drops of glacial acetic acid. Simultaneously, 4-aminoantipyrine (2.03 g, 0.01 mol) was dissolved in 25 mL of absolute ethanol under continuous stirring. The mixture was then refluxed for 8 h, followed by cooling and collection. Recrystallization was performed by removing unreacted material using 98% ethanol. The resulting product was collected and weighed for use in the second step, yielding an 85% productivity. The nano ligand (1E,2E)-N1, N2-bis((Z)-1,5-dimethyl-2-phenyl-3-(thiazol-5-ylimino)-2,3-dihydro-1H-pyrazol-4-yl)-1,2-diphenylethane-1,2-diimine (NPTIPPE) was then prepared by dissolving compound-A (2.86 g, 0.01 mol) in 25 mL of absolute ethanol with continuous stirring and adding 4-5 drops of glacial acetic acid. Separately, 2-aminothiazole (2 g, 0.02 mol) was dissolved in 25 mL of absolute ethanol. The solutions were mixed together and refluxed for 8 h. The mixture was cooled, and the resulting precipitate was filtered and dried. Recrystallization from absolute ethanol yielded a product with an 81% yield and a melting point of 120°C, as illustrated in Fig. 1.

Synthesis of the complex

The complex was prepared in a 1:1 ratio using a standard method. A solution of the nano ligand (NPTIPPE) (0.37 g, 0.001 mol) in 10 mL of ethanol was mixed with palladium chloride ($PdCl_2$) (0.18 g, 0.001 mol) in 10 mL of absolute ethanol. The mixture was refluxed for 2 h with continuous

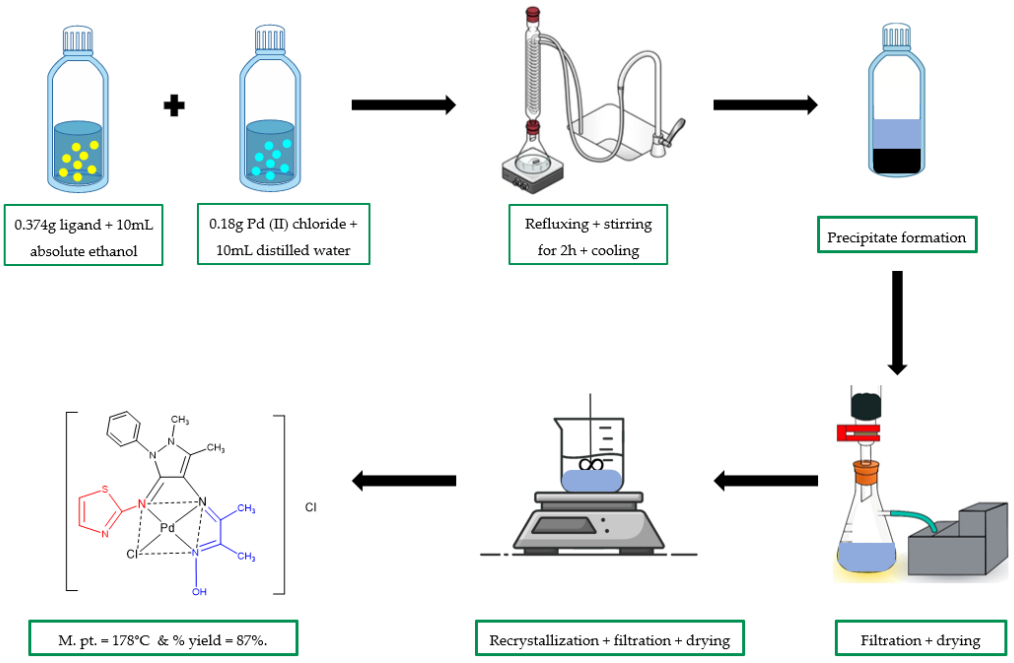

Fig. 2. Schematic illustration for the synthesis of Pd (II) complex by novel Schiff base nano ligand (NPTIPPE).

Table 1. Elemental analysis and some physical properties of the nano ligand (NPTIPPE) and its metallic complex.

Compound (Chemical Formula)	Color	M.P (°C)	Yield %	M.W (g/mol)	Calc. (Found)%				
					C	H	N	Pd	
Ligand (NPTIPPE) $C_{18}H_{20}N_6OS$	Dark golden	120	81	744.94	67.72 68.73	4.87 4.93	18.80 19.34	----- -----	----- -----
[Pd (NPTIPPE)Cl]Cl $C_{18}H_{20}Cl_2N_6OPdS$	Brown	173	72	922.26	54.70 55.51	3.93 4.12	15.19 15.93	11.54 12.17	19.50 (20.17)

stirring. It was then cooled, filtered, and dried before being recrystallized using absolute ethanol to obtain a pure complex. The yield was 72%, with a melting point of 173℃ (Fig. 2).

Cell toxicity tests: cell lines and cultivation of MCF-7 breast cancer cell line

In this study, two cell lines were utilized: the breast cancer cell line (MCF-7) and the normal human liver cell line (WRL-68). The cell lines were stored in liquid nitrogen, maintained and tested at the Division of Cellular, Molecular, Microbial, and Animal Services / Roshdy Azmeh Company in Tehran. After preparing the cancer cell line suspensions (MCF-7) at a concentration of 1×10^{-5} cells/well, the cell suspension was placed in a 96-well flat-bottom plate and incubated under appropriate conditions in an incubator containing 5% carbon dioxide (CO_2) at 37℃ for 24 h. Subsequently, 100 µL of this suspension was added to each well. The prepared concentrations of the ligands and the Pd (II) complex—10, 25, 50, 100, 250, and 500 µg/mL—were then added to the wells, with three wells per concentration. The plate was then incubated for 24 h at 37℃. Following this incubation, 10 µL of MTT solution at a concentration of 0.45 mg/mL was added to each well, and the plate was incubated for an additional 4 h at 37℃. Afterward, 100 µL of a DMSO solution was introduced into each well and left to incubate for duration of 5 min. Ultimately, the samples' absorbance was measured at a wavelength of 570 nm utilizing an ELISA reader. Subsequent statistical analysis was conducted on the optical density measurements in order to get the IC50 value.

RESULTS AND DISCUSSION

The novel nano ligand (NPTIPPE) was synthesized through the sequential reaction of benzil with 4-aminoantipyrine and 2-aminothiazole. The Pd (II) complex was prepared by reacting the nano ligand (NPTIPPE) with palladium chloride dissolved in ethanol. Table 1 presents the physical properties and elemental analysis of both the ligand and its complex. The palladium complex was prepared in a 1:1 of metal:ligand ratio.

NMR spectrum of the novel Schiff base ligand (NPTIPPE)

Fig. 3 illustrates the ^{1}H-NMR spectrum of the ligand (NPTIPPE). The ^{1}H-NMR spectrum of the ligand (NPTIPPE) exhibited two singlets at δ = 2.13 ppm (S, 3H) and δ = 3.16 ppm (S, 3H), corresponding to the protons of the methyl groups (C-CH_3 and N-CH_3) on the pyrazole ring, respectively [10]. Additional multiple signals were observed at δ = 7.18 - 7.69 ppm (M, 10H), attributed to the protons of the phenyl rings on the pyrazole and benzyl moieties [11]. The protons on the thiazole ring produced a doublet at δ = 7.72 and 7.75 ppm (d, 2H) [12].

^{13}C-NMR spectrum of the ligand (NPTIPPE)

The ^{13}C-NMR spectrum of the ligand (NPTIPPE) showed a signal at 40.35 ppm due to DMSO. A signal at 10.43 ppm was observed (Fig. 4), corresponding to the carbon atoms (C8 and C39) of the methyl groups (-CH_3) attached to the pyrazole

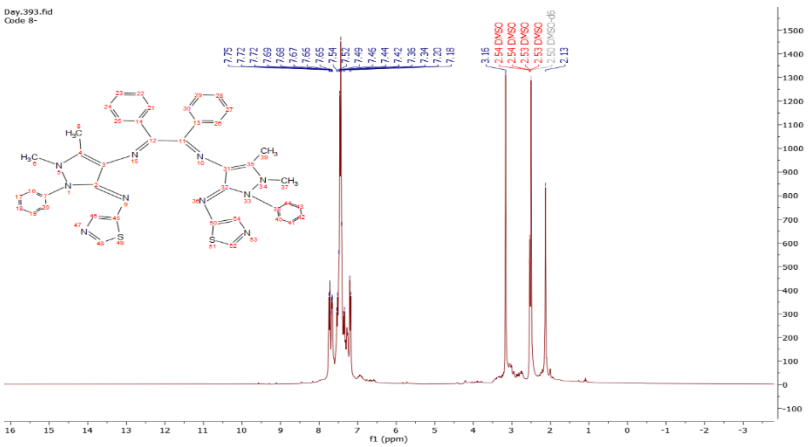

Fig. 3. ^{1}H-NMR result of the (NPTIPPE) ligand.

ring. The carbon C6 and C37 atoms gave a signal at 35.29 ppm, indicating the methyl group attached to the nitrogen of the pyrazole ring [13]. A signal at 106.49 ppm was attributed to the carbon atoms C3 and C31 of the pyrazole ring. Additionally, a signal at 138.63 ppm was associated with the carbon atoms C4 and C35 of the pyrazole ring containing the methyl group (-CH_3) [14]. Signals at 116.34 ppm were attributed to the carbon atoms C45 and C50, while signals at 137.16 ppm corresponded to the carbon atoms C46 and C54, and signals at 192.81 ppm were associated with the carbon atoms C48 and C52 of the thiazole ring [15, 16]. The following carbon atoms: C7, C13, C14, C16, C18, C20, C21, C22, C23, C24, C25, C27, C28, C29, C30, C38, C40, C42, and C44, gave values ranging between 124.12 ppm and 135.46 ppm, indicating the phenyl rings attached to the azomethine group and the phenyl ring attached to the nitrogen of the pyrazole ring [16]. A signal at 152.08 ppm was attributed to the carbon atoms C12 and C11, while another signal at 154.35 ppm corresponded to the carbon atoms C2 and C35 of the azomethine groups [17-20].

FT-IR results

The ligand (NPTIPPE) had several IR bands (Fig. 5). The bands seen at 3055 cm^{-1} and 3031 cm^{-1} can be attributed to aromatic (C-H) groups, while the bands at 2908 cm^{-1} and 2815 cm^{-1} correspond to aliphatic (C-H) groups [21-24]. A well-defined absorption band at 1658 cm^{-1} indicated ligand production and confirmed the azomethine (C=N) group. The 1589 cm^{-1} band indicated the azomethine (C=N) group in the thiazole ring [25, 26]. The aromatic (C=C) groups and thiazole ring (C-S) are indicated by absorption bands at 1558 cm^{-1}, 1488 cm^{-1}, and 1134 cm^{-1} [27-29].

The FTIR spectrum of the palladium (II) complex (Fig. 6) shows that coordination and complex formation shifted several absorption bands in the free ligand spectrum to lower frequencies. This shift strongly suggests complex development. The azomethine group changed from 1658 cm^{-1} in the ligand spectrum to 1635 cm^{-1} in the complex spectrum [30-34]. The M-N group also produced a 594 cm^{-1} [35-37]. Table 2 shows the ligand (NPTIPPE) and palladium (II) complex FTIR bands.

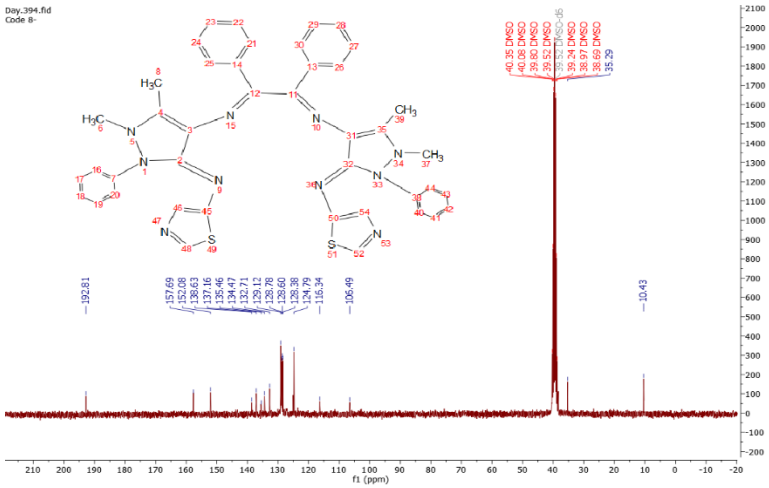

Fig. 4. ^{13}C-NMR spectrum of the NPTIPPE ligand.

Table 2. The significant ligand (NPTIPPE) and palladium (II) complex spectral bands.

Compound	υ (C-H) Arom. υ (C-H) Aliph.	υ(C=N) Imine	υ(C=N) Thiazole	υ(C=C) aromatic	υ(M-N)
Ligand (NPTIPPE)	3055, 3031 2908, 2815	1658	1589	1558 1488	-
[Pd(NPTIPPE)]Cl_2	3062 2977, 2908	1635	1573	1558 1488	594

UV-visible results

The UV-Vis spectrum of the nano ligand (NPTIPPE) exhibited two peaks, as shown in Fig. 7 and Table 3. The first peak, centered at 243 nm (41152 cm^{-1}), corresponds to the (π-π*) transition, while the second peak, at 320 nm (31153 cm^{-1}), is attributed to the (n-π*) transition of the azomethine group [35, 38, 39]. In the UV-Vis spectrum of the palladium (II) complex (Fig. 8), several absorption peaks were observed at 252 nm (39683 cm^{-1}) and 341 nm (29326 cm^{-1}), indicating intra-ligand transitions. Three additional absorption peaks appeared at 478 nm (20921 cm^{-1}), 508 nm (19685 cm^{-1}), and 536 nm (18657 cm^{-1}), corresponding to the electronic transitions $^1A_1g \rightarrow {}^1Eg$, $^1A_1g \rightarrow {}^1B_1g$, and $1A_1g \rightarrow {}^1A_2g$, respectively, confirming the square planar geometry of the complex [40]. Magnetic susceptibility measurements indicated that the complex exhibits diamagnetic properties [41].

Molar conductivity measurements

Molar conductivity measurements were prepared using absolute ethanol at a concentration of $1x10^{-3}$ M at room temperature. These measurements indicated that the prepared complex has a molar conductivity value of 73.98 ohm^{-1} cm^2 $mol^{-1,}$ suggesting that the complex possesses ionic characteristics with a 1:2 ratio [42].

XRD analysis

A solid-state XRD study examined the crystal structure [22, 23] of NPTIPPE and its metal complexes in the 2θ=5-80 range. This investigation measured crystal structure, crystallite size, macrostrains, and dislocation density to determine

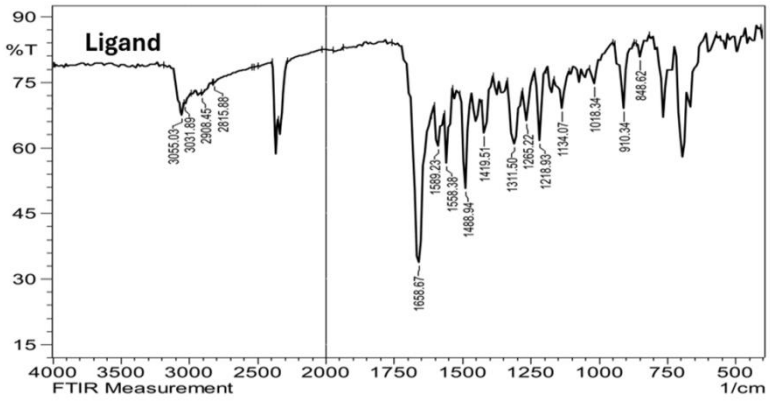

Fig. 5. FTIR spectrum of the NPTIPPE ligand.

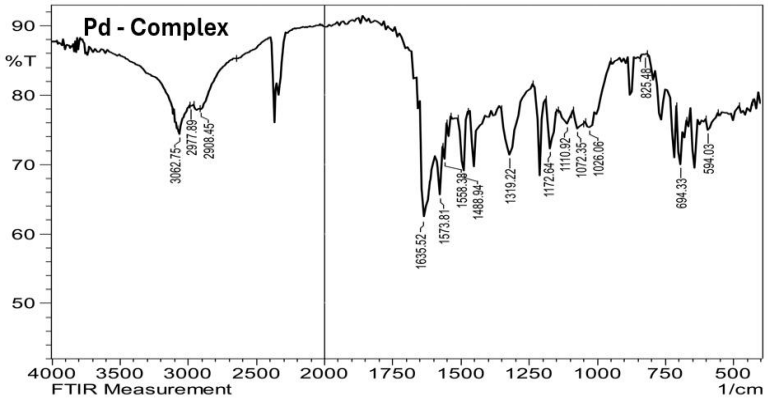

Fig. 6. FTIR spectrum of the Pd (II) complex.

purity and defects when the ligand is transformed into the palladium complex. Micro-strains such lattice deformation and crystal fracture due to crystal distortions, crystallite size, and distribution cause some diffraction peaks [43-47]. The synthesized ligand's XRD pattern displayed strong peaks, indicating a crystalline network. In contrast, the palladium complex had broad peaks,

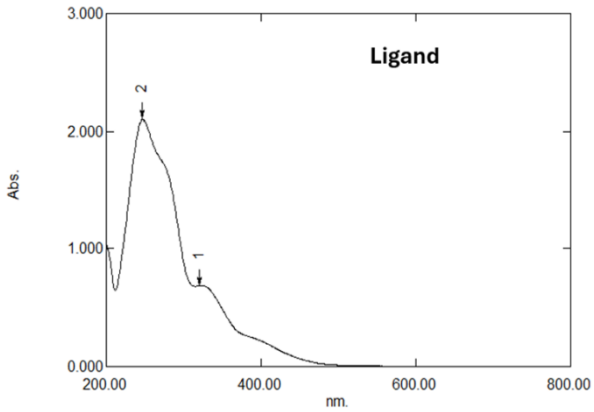

Fig. 7. UV-visible spectrum of the NPTIPPE ligand.

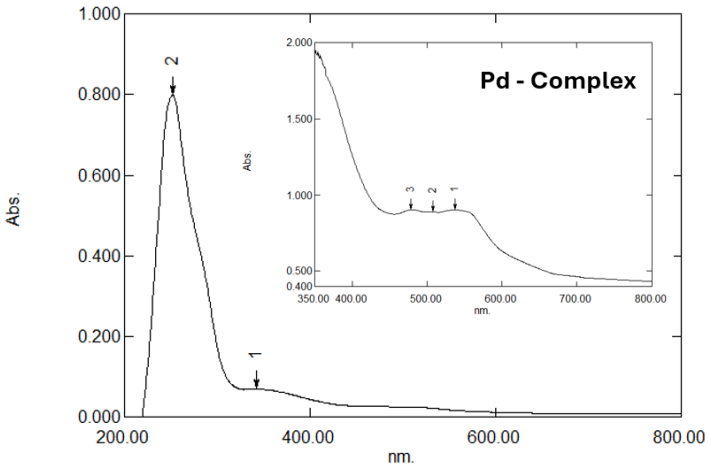

Fig. 8. UV-visible spectrum of the Pd (II) complex.

Table 3. Peaks absorption values, magnetic momentum and expected geometry for nano ligand (NPTIPPE) and Pd(II) complex.

Compounds	λ (nm)	υ (cm^{-1})	Transitions	μeff (B.M)	Geometry
Nano ligand (NPTIPPE)	243 321	41152 31153	π-π* n-π*	-	-
[Pd (NPTIPPE)]Cl_2	252 341 478 508 536	39683 29326 20921 19685 18657	Intra Ligand Intra Ligand $^1A_1g \rightarrow {}^1Eg$ $^1A_1g \rightarrow {}^1B_1g$ $^1A_1g \rightarrow {}^1A_2g$	(Dia.)	Square planar dsp^2

indicating amorphous structures. The sharpness of the peaks depends on the crystalline order, lattice properties, and crystal planes. Debye-Scherrer's equation was used to calculate the crystallite size of the nano ligand (NPTIPPE) and the palladium complex:

$$D = \frac{k\,\lambda}{\beta \cos \theta} \quad (1)$$

To calculate the dislocation density, the following equation is commonly used:

$$\delta = 1/D^2 \quad (2)$$

By analyzing the XRD patterns, significant differences in crystallite size, dislocation density, and interplanar spacing (d-spacing) between the nano ligand (NPTIPPE) and the prepared palladium complex were observed. These differences confirm the coordination process between the ligand and the palladium ion [48, 49]. In Fig. 9 and Table 4, a comparison of the intensity and positions of the obtained peaks with standard reference cards indicates that these peaks correspond to the original compounds from which the complexes were derived. However, there were also unusual peaks that did not match any known substances, suggesting that the compounds are new and have not been compared with various global standards [50]. Utilizing the XRD data, it was concluded that the prepared materials exhibit nanomaterial

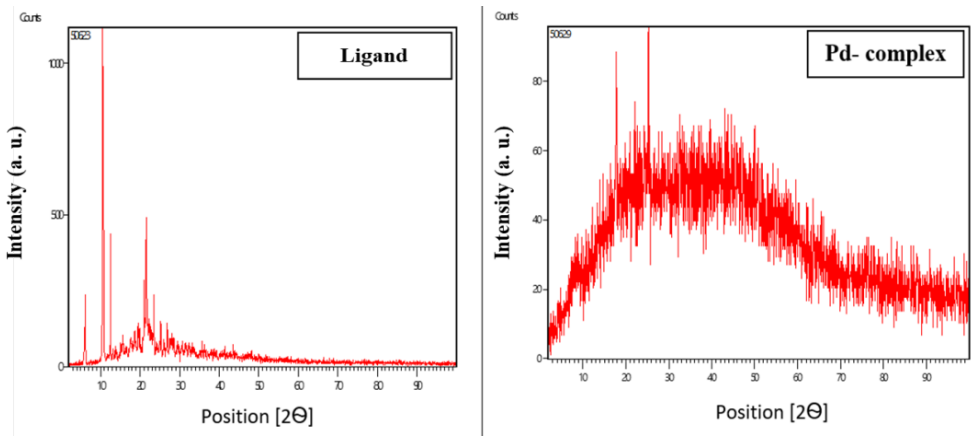

Fig. 9. XRD patterns of nano ligand (NPTIPPE) and Pd (II) complex.

Table 4. Summary of the information obtained from the XRD analysis i.e., diffraction angles, d-spacing, and relative intensities for ligand (NPTIPPE) and its Pd (II) complex.

Compound	No.	*Peak* Position °2Θ	d-spacing (Å)	Rel.Int. [%]	FWHM	Width	Crystallite Size. (nm)	Lattice Strain
Nano ligand (NPTIPPE)	1	0.04	0.18	17.93	0.18	0.09	44.20	0.04
	2	0.08	0.21	100.00	0.21	0.10	38.54	0.08
	3	0.04	0.08	34.06	0.08	0.04	98.67	0.04
	4	0.26	0.32	35.15	0.32	0.16	25.35	0.26
	5	0.18	0.19	18.98	0.19	0.10	41.82	0.18
[Pd(NPTIPPE)]Cl_2	1	0.22	0.32	93.86	0.32	0.16	24.97	0.22
	2	22.01	0.16	78.43	0.16	0.08	50.90	0.13
	3	25.22	0.23	100.00	0.23	0.12	35.24	0.23
	4	43.08	0.22	56.17	0.22	0.11	39.54	0.37
	5	50.04	0.16	69.48	0.16	0.08	55.49	0.32

characteristics [51-53].

Scanning electron microscopy (FE-SEM)

As shown in Fig. 10, the surface investigations of resulting NPTIPPE and pd(II) complex possess smooth shapes. It should be noted that Pd-complex reveals an interconnected structures as compared with NPTIPPE ligand.

Anticancer activity

The synthesized NPTIPPE and Pd(II) complex were evaluated for MTT on the most prevalent cancer cell line (MCF-7) (Figs. 11-14). To determine their therapeutic potential, NPTIPPE and Pd(II) complex were evaluated on healthy WRL-68 liver cells. Following 24 h of incubation at 37°C, the MTT assay was performed at doses of 0, 10, 25, 50, 100, 250, and 500 µg/mL. The NPTIPPE effectively inhibited MCF-7 cancer and WRL-68 healthy cell growth, with the lowest inhibition at 10 µg/mL and the maximum at 500 µg/mL. The proportion of viable MCF-7 and WRL-68 cells after ligand contact ranged from 4.35924% to 92.94909% and 60.57843% to 99.06862%, respectively. Maximum MCF-7 cell inhibition was 95.64072% at 500 µg/mL, while WRL-68 cells showed 39.42157% inhibition. The ligand produced an IC50 value of 78.56 µg/mL for MCF-7 cells and 220.84 µg/mL for WRL-68

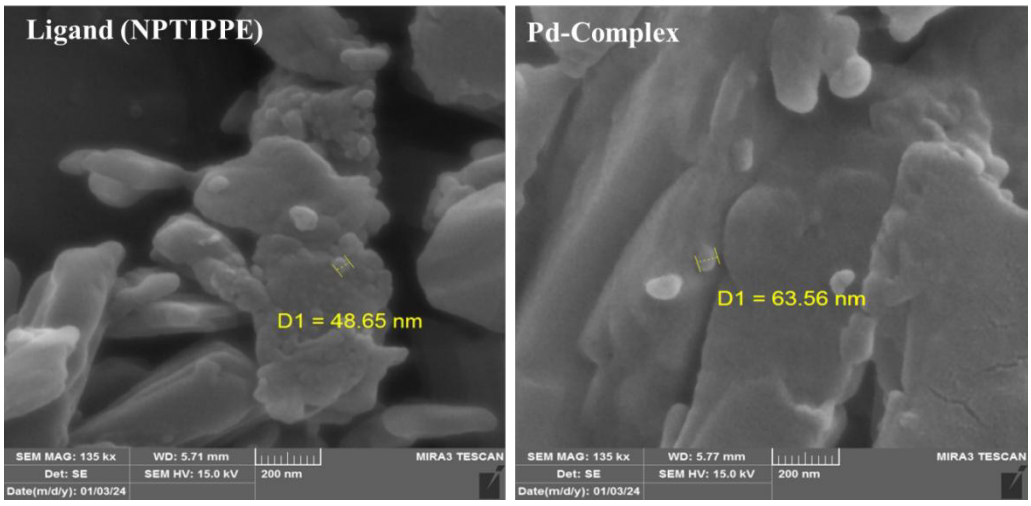

Fig. 10. The FESEM images of the synthesized NPTIPPE and Pd (II) complex.

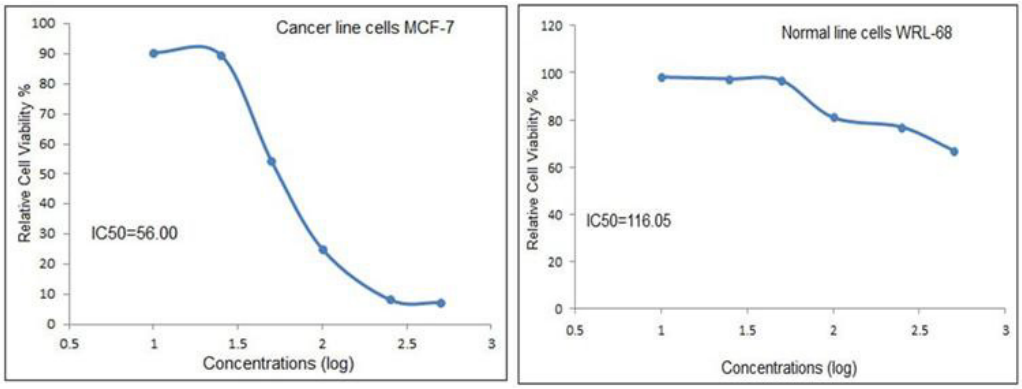

Fig. 11. The relationship between the biological activity of MCF-7 breast cancer cell line and WRL-68 normal cell line against the concentration of the ligand (NPTIPPE).

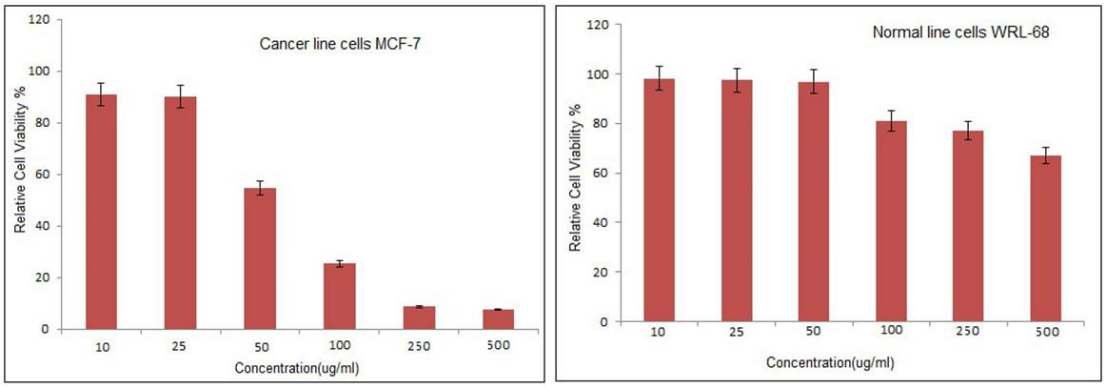

Fig. 12. Comparison of living cells at selected concentrations of the MCF-7 breast cancer cell line and WRL-68 normal cell line for the ligand (NPTIPPE).

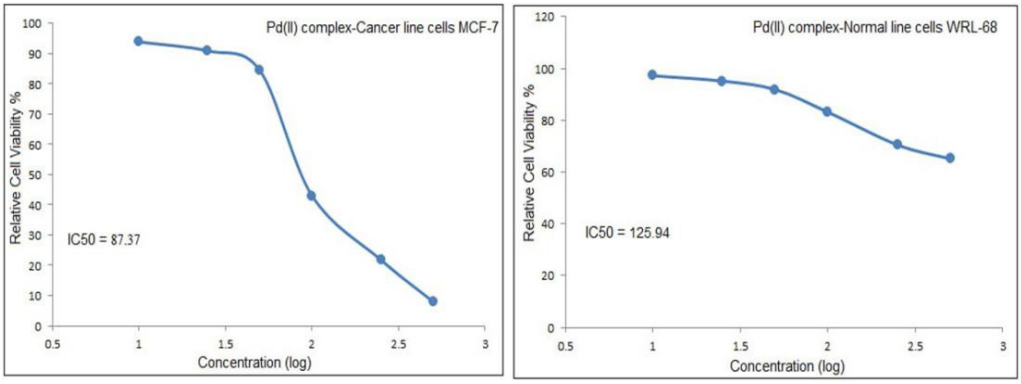

Fig. 13. The relationship between the biological activity of MCF-7 breast cancer cell line and WRL-68 normal cell line against the concentration of the Pd(II) complex.

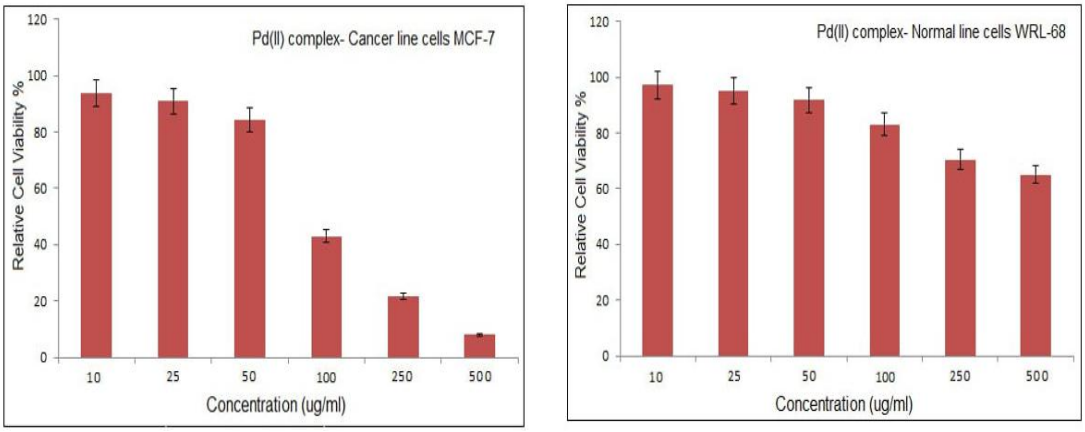

Fig. 14. Comparison of living cells at selected concentrations of the MCF-7 breast cancer cell line and WRL-68 normal cell line for the Pd(II) complex.

Table 5. Evaluation of the cytotoxicity of both the nano ligand against the MCF-7 cancer cell line and WRL-68 cell line after incubation (24 h) at 37 °C.

Concentration (μg/mL)	HL					
	Cancer line cells MCF-7			Normal line cells WRL-68		
	Cell Viability		%Cell inhibition	Cell Viability		%Cell inhibition
	Mean	SD		Mean	SD	
10	92.949	4.029	7.051	99.069	1.274	0.931
25	91.486	2.291	8.514	98.549	15.958	1.451
50	79.111	8.620	20.889	96.608	3.571	3.392
100	35.709	4.274	64.291	78.578	0.516	21.422
250	21.781	3.616	78.219	75.412	4.710	24.588
500	4.359	0.101	95.641	60.578	5.148	39.422
IC50		78.56			220.84	

Table 6. Evaluation of the cytotoxicity of the Pd(II) complex against the MCF-7 cancer cell line and WRL-68 cell line after incubation (24 h) at 37 °C.

Concentration (μg/mL)	Pd(II) complex					
	Cancer line cells MCF-7			Normal line cells WRL-68		
	Cell Viability		%Cell inhibition	Cell Viability		%Cell inhibition
	Mean	SD		Mean	SD	
10	93.89225	5.13964	6.10775	97.18371	5.02897	2.81629
25	90.92106	7.29320	9.07894	95.1072	9.23502	4.8928
50	84.40449	1.69457	15.59551	91.85799	6.64557	8.14201
100	42.99023	4.25257	57.00977	83.13108	1.27947	16.86892
250	21.79632	3.64183	78.20368	70.47864	9.65738	29.52136
500	7.98046	0.99631	92.01954	65.07944	8.18448	34.92056
IC50		87.37			125.94	

cells. The proliferation of MCF-7 cancer cells and WRL-68 healthy cells was inhibited by the Pd(II) complex of the NPTIPPE at concentrations ranging from 10 μg/mL to 500 μg/mL. After interaction with the Pd(II) complex, MCF-7 cells had 7.98046% to 93.89225% vitality and WRL-68 cells 65.07944% to 97.18371%. The maximum inhibition of MCF-7 cells was 92.01954% at 500 μg/mL, while WRL-68 cells showed 34.92056% inhibition. IC50 values for palladium complex interaction with MCF-7 and WRL-68 cells were 87.37 and 125.94 μg/mL, respectively (Table 5 and Table 6).

CONCLUSION

In this study, a novel ligand (NPTIPPE) derived from antipyrine was synthesized in two steps, followed by the preparation of its palladium complex. Various methods were employed, including spectroscopic techniques (FTIR spectroscopy, UV-Vis. spectroscopy, and NMR spectroscopy), atomic absorption, FESEM, XRD, and physical methods (melting point, molar conductivity, elemental analysis) to confirm the structure of the synthesized NPTIPPE and its complex. The FTIR spectrum showed that the ligand coordinates with the Pd (II) ion through the four nitrogen atoms of the azomethine groups, indicating that the ligand acts as a tetradentate ligand. This coordination results in a square planar geometry for the complex. MTT assays were conducted for both NPTIPPE and its palladium complex on cancerous and healthy cells. The palladium complex was found to be more effective against breast cancer cells (MCF-7) than the nano ligand itself, suggesting that the palladium complex holds significant potential as a therapeutic agent.

CONFLICT OF INTEREST

The authors declare that there is no conflict of interests regarding the publication of this manuscript.

REFERENCES

1. Zhang Z-H; Wu H-M; Deng S-N; Cai X-Y; Yao Y; Mwenda MC; Wang J-Y; Cai D; Chen Y. Design, Synthesis, and Anticancer Activities of Novel 2-Amino-4-phenylthiazole Scaffold Containing Amide Moieties. Journal of Chemistry.

2018;2018(1):4301910.
2. Mishra CB; Kumari S; Tiwari M. Thiazole: A promising heterocycle for the development of potent CNS active agents. European journal of medicinal chemistry. 2015;92:1-34.
3. Mohanram I; Meshram J. Synthesis and Biological Activities of 4-Aminoantipyrine Derivatives Derived from Betti-Type Reaction. International Scholarly Research Notices. 2014;2014(1):639392.
4. Forer A; Fabian L. Does 2, 3-butanedione monoxime inhibit nonmuscle myosin? Protoplasma. 2005;225:1-4.
5. Elgazar SM; Abd El-Karim AT; Mahmoud WH; El-Sherif AA. Comprehensive Analysis of Nitrogen–Oxygen Schiff Base Derived from Triazole and Its Metal Complex: Synthesis, Structural Characterization, and Biological Activities with Theoretical Insights for Anti-Helicobacter pylori, Antitumor, and Anti-COVID-19 Applications. Egyptian Journal of Chemistry. 2025;68(3):169-191.
6. Naglah AM; Almehizia AA; Al-Wasidi AS; Alharbi AS; Alqarni MH; Hassan AS; Aboulthana WM. Exploring the potential biological activities of pyrazole-based schiff bases as anti-diabetic, anti-Alzheimer's, anti-inflammatory, and cytotoxic agents: in vitro studies with computational predictions. Pharmaceuticals. 2024;17(5):655.
7. Mandal S; Sarkar M; Denrah S; Bagchi A; Biswas A; Cordes DB; Slawin AM; Saha NC. Catalytic and anticancer activity of two new Ni (II) complexes with a pyrazole based heterocyclic Schiff-base ligand: Synthesis, spectroscopy and X-ray crystallography. Journal of Molecular Structure. 2023;1287:135648.
8. Hosny S; Ragab MS; Abd El-Baki RF. Synthesis of a new sulfadimidine Schiff base and their nano complexes as potential anti-COVID-19 and anti-cancer activity. Scientific Reports. 2023;13(1):1502.
9. Mahmoud WH; Omar M; Sayed FN; Mohamed GG. Synthesis, characterization, spectroscopic and theoretical studies of transition metal complexes of new nano Schiff base derived from L-histidine and 2-acetylferrocene and evaluation of biological and anticancer activities. Applied Organometallic Chemistry. 2018;32(7):e4386.
10. Shaker SA. Preparation and Spectral Properties of Mixed-Ligand Complexes of VO (IV), Ni (II), Zn (II), Pd (II), Cd (II) and Pb (II) with Dimethylglyoxime and N-acetylglycine. Journal of Chemistry. 2010;7:S580-S586.
11. Hamad K; Kaseem M; Deri F. Recycling of waste from polymer materials: An overview of the recent works. Polymer degradation and stability. 2013;98(12):2801-2812
12. Sun Y-S; Zhao Z; Yang Z-N; Xu F; Lu H-J; Zhu Z-Y; Shi W; Jiang J; Yao P-P; Zhu H-P. Risk factors and preventions of breast cancer. International journal of biological sciences. 2017;13(11):1387.
13. Porock D. Predicting the severity of radiation skin reactions in women with breast cancer. 1998.
14. Sharma GN; Dave R; Sanadya J; Sharma P; Sharma K. Various types and management of breast cancer: an overview. Journal of advanced pharmaceutical technology & research. 2010;1(2):109-126.
15. Saini A; Kumar M; Bhatt S; Saini V; Malik A. Cancer causes and treatments. Int J Pharm Sci Res. 2020;11(7):3121-3134
16. Abd Alkareem T; Hassan S; Abdalhadi S. Breast cancer: symptoms, causes, and treatment by metal complexes: a review. Advanced Journal of Chemistry-Section B: Natural Products and Medical Chemistry. 2023;5(4):306-319.
17. Beran JA. Laboratory manual for principles of general chemistry: John Wiley & Sons; 2010.
18. Firuzabadi FD; Asadi Z; Yousefi R. Synthesis of new nano Schiff base complexes: X-ray crystallography, thermal, electrochemical and anticancer studies of nano uranyl Schiff base complexes. Bulletin of the Chemical Society of Ethiopia. 2018;32(1):89-100.
19. El Tabl A; Abd Wlwahed M; Abd-Elwareth M; Faheem S. Nano metal complexes in cancer therapy, preparation, spectroscopic, characterization and anti-breast cancer activity of new metal complexes of alanine Schiff-base. Egyptian Journal of Chemistry. 2021;64(6):3131-3152.
20. Carroll FA. Perspectives on structure and mechanism in organic chemistry: John Wiley & Sons; 2023.
21. Roy M; Biswas J; Datta A. Breast cancer: epidemiology, types, diagnosis, and treatment. Genetics and epigenetics of breast cancer: Springer; 2023. p. 1-24.
22. Obeagu EI; Obeagu GU. Breast cancer: A review of risk factors and diagnosis. Medicine. 2024;103(3):e36905.
23. Grimsey E. An overview of the breast and breast cancer. Breast Cancer Nursing Care and Management. 2010:1-18
24. Spinu C; Kriza A. Co (II), Ni (II) and Cu (II) complexes of bidentate Schiff bases. Acta Chimica Slovenica. 2000;47(2):179-186.
25. Khan M; Khan A; Hussain I; Khan MA; Gul S; Iqbal M; Khuda F. Spectral, XRD, SEM and biological properties of new mononuclear Schiff base transition metal complexes. Inorganic Chemistry Communications. 2013;35:104-109.
26. Refat MS; El-Sayed MY; Adam AMA. Cu (II), Co (II) and Ni (II) complexes of new Schiff base ligand: Synthesis, thermal and spectroscopic characterizations. Journal of Molecular Structure. 2013;1038:62-72.
27. Dubey RK; Baranwal P. Synthesis, Reactions and Spectroscopic {UV-Visible, IR, NMR (1H-& 13C-), FAB-MS, TGA and XRD} Studies of New Mercury (II) Complexes Containing Various Mixed Ligand Schiff Bases. Main Group Metal Chemistry. 2009;32(6):321-340.
28. Mohamed GG; Omar M; Ibrahim AA. Biological activity studies on metal complexes of novel tridentate Schiff base ligand. Spectroscopic and thermal characterization. European journal of medicinal chemistry. 2009;44(12):4801-4812.
29. El-Sonbati A; Mahmoud W; Mohamed GG; Diab M; Morgan SM; Abbas S. Synthesis, characterization of Schiff base metal complexes and their biological investigation. Applied Organometallic Chemistry. 2019;33(9):e5048.
30. Lastovickova M; Strouhalova D; Bobalova J. Use of lectin-based affinity techniques in breast cancer glycoproteomics: a review. Journal of proteome research. 2020;19(5):1885-1899.
31. Numan HRHAW. BIOCHEMICAL, STUDY ON SUPEROXIDE DISMUTASE ENZYMIE IN PATIENTS WITH DIFFERENT BRAIN.
32. de Araujo EL; Barbosa HFG; Dockal ER; Cavalheiro ÉTG. Synthesis, characterization and biological activity of Cu (II), Ni (II) and Zn (II) complexes of biopolymeric Schiff bases of salicylaldehydes and chitosan. International journal of biological macromolecules. 2017;95:168-176.
33. Hansen S; Thiel S; Willis A; Holmskov U; Jensenius JC. Purification and characterization of two mannan-binding lectins from mouse serum. The Journal of Immunology. 2000;164(5):2610-2618.
34. Yehia SM; Ayoub IM; Watanabe M; Devkota HP; Singab ANB. Metabolic profiling, antioxidant, and enzyme inhibition

potential of Iris pseudacorus L. from Egypt and Japan: A comparative study. Scientific Reports. 2023;13(1):5233.
35. Hine J; Yeh CY. Equilibrium in formation and conformational isomerization of imines derived from isobutyraldehyde and saturated aliphatic primary amines. Journal of the American Chemical Society. 1967;89(11):2669-2676.
36. Sacarescu L; Ardeleanu R; Sacarescu G; Simionescu M. Highly Crosslinked Polysilane–Schiff Base. Polymer Bulletin. 2005;54(1):29-37.
37. Shakir M; Hanif S; Sherwani MA; Mohammad O; Al-Resayes SI. Pharmacologically significant complexes of Mn (II), Co (II), Ni (II), Cu (II) and Zn (II) of novel Schiff base ligand,(E)-N-(furan-2-yl methylene) quinolin-8-amine: Synthesis, spectral, XRD, SEM, antimicrobial, antioxidant and in vitro cytotoxic studies. Journal of Molecular Structure. 2015;1092:143-159.
38. Saheb V; Sheikhshoaie I; Stoeckli-Evans H. A novel tridentate Schiff base dioxo-molybdenum (VI) complex: Synthesis, experimental and theoretical studies on its crystal structure, FTIR, UV–visible, 1H NMR and 13C NMR spectra. Spectrochimica Acta Part A: Molecular and Biomolecular Spectroscopy. 2012;95:29-36.
39. Shelke V; Jadhav S; Patharkar V; Shankarwar S; Munde A; Chondhekar T. Synthesis, spectroscopic characterization and thermal studies of some rare earth metal complexes of unsymmetrical tetradentate Schiff base ligand. Arabian journal of chemistry. 2012;5(4):501-507.
40. Sheikhshoaie I; Saheb V. A new salen base 5-(phenylazo)-N-(2-amino pyridine) salicyliden Schiff base ligand: Synthesis, experimental and density functional studies on its crystal structure, FTIR, 1H NMR and 13C NMR spectra. Spectrochimica Acta Part A: Molecular and Biomolecular Spectroscopy. 2010;77(5):1069-1076.
41. Oladeji OS; Ikhile MI; Ojo O; Fotsing CM; Mamo M; Ndungu PG; Ndinteh DT. Synthesis, FTIR, NMR, UV–vis and electrochemistry analysis of ferrocenyl Schiff bases. Inorganica Chimica Acta. 2023;546:121319.
42. Kavitha N; Lakshmi PA. Synthesis, characterization and thermogravimetric analysis of Co (II), Ni (II), Cu (II) and Zn (II) complexes supported by ONNO tetradentate Schiff base ligand derived from hydrazino benzoxazine. Journal of Saudi Chemical Society. 2017;21:S457-S466.
43. David ST; Priyadharsini J. SCHIFF BASE LIGAND ITS COMPLEXES AND THEIR FT-IR SPECTROSCOPY STUDIES. International Journal on Applied Bioengineering. 2015;9(1)
44. Ahmadi RA; Amani S. Synthesis, spectroscopy, thermal analysis, magnetic properties and biological activity studies of Cu (II) and Co (II) complexes with Schiff base dye ligands. Molecules. 2012;17(6):6434-6448.
45. Osypiuk D; Cristóvão B; Bartyzel A. New coordination compounds of CuII with Schiff base ligands—Crystal structure, thermal, and spectral investigations. Crystals. 2020;10(11):1004.
46. Maddila S; Gorle S; Seshadri N; Lavanya P; Jonnalagadda SB. Synthesis, antibacterial and antifungal activity of novel benzothiazole pyrimidine derivatives. Arabian Journal of Chemistry. 2016;9(5):681-687.
47. Pluth MD; Tonzetich ZJ. Hydrosulfide complexes of the transition elements: diverse roles in bioinorganic, cluster, coordination, and organometallic chemistry. Chemical Society Reviews. 2020;49(12):4070-4134
48. Jiang J; Tang X; Dou W; Zhang H; Liu W; Wang C; Zheng J. Synthesis and characterization of the ligand based on benzoxazole and its transition metal complexes: DNA-binding and antitumor activity. Journal of Inorganic Biochemistry. 2010;104(5):583-591.
49. Yaul AR; Dhande VV; Pethe GB; Aswar AS. Synthesis, characterization, biological and electrical conductivity studies of some Schiff base metal complexes. Bulletin of the Chemical Society of Ethiopia. 2014;28(2):255-264.
50. Mohanan K; Subhadrambika N; Joseyphus RS; Swathy S; Nisha V. Synthesis, spectroscopic characterization, solid state dc electrical conductivity and biological studies of some lanthanide (III) chloride complexes with a heterocyclic Schiff base ligand. Journal of Saudi Chemical Society. 2016;20(4):379-390.
51. Mekhalif Z; Fonder G; Auguste D; Laffineur F; Delhalle J. Impact of the anchoring groups X (–SH,–S–S–,–SeH and–Se–Se–) of CF3 (CF2) 3 (CH2) 11X molecules self-assembled on oxidised electroplated copper. Journal of Electroanalytical Chemistry. 2008;618(1-2):24-32.
52. Venugopala KN; Chandrashekharappa S; Pillay M; Bhandary S; Kandeel M; Mahomoodally FM; Morsy MA; Chopra D; Aldhubiab BE; Attimarad M. Synthesis and structural elucidation of novel benzothiazole derivatives as anti-tubercular agents: In-silico screening for possible target identification. Medicinal Chemistry. 2019;15(3):311-326.
53. Issa Y; Hassib H; Abdelaal H. 1H NMR, 13C NMR and mass spectral studies of some Schiff bases derived from 3-amino-1, 2, 4-triazole. Spectrochimica Acta Part A: Molecular and Biomolecular Spectroscopy. 2009;74(4):902-910.